Journal of Molecular Modeling (2022) 28: 98
https://doi.org/10.1007/s00894-022-05088-w

ORIGINAL PAPER

DFT analysis of valproic acid adsorption onto Al_{12}/B_{12}-N_{12}/P_{12} nanocages with solvent effects

Jamelah S. Al-Otaibi[1] · Y. Sheena Mary[2] · Y. Shyma Mary[2]

Received: 19 January 2022 / Accepted: 11 March 2022 / Published online: 23 March 2022

Abstract
Using density functional theory, the adsorption of valproic acid onto the surface of fullerene-like nanocages was investigated. Valproic acid interacts with the nanocages through the carboxylic group with energies of − 144.14, − 109.71, − 105 .22, and − 84.96 kcal/mol. The frontier molecular orbital (FMO) energy levels were considerably altered upon adsorption, resulting in a reduction in energy gap and increase in electrical conductivity. This suggests that nanocages could be used as sensors as well as options for drug administration in biological systems. Solvation effects in water are also reported.

Keywords DFT · Valproic acid detection · Solvation · Adsorption · Sensor · Biosensor · Nanocages

Introduction

The impact of nanotechnology on industry and medicine is enormous [1, 2]. Advancements in numerous sectors of research, including microscopic particles and nano-structured materials, have been made in recent years [3–8]. Currently, a variety of types are available for the development of sensors and drug carriers [9–12]. The properties of the drug-nanostructure complex undergo changes as a result of the electron exchange between the adsorbed molecules and the nanomaterials, which can be monitored as a possible sensor [6, 7, 13, 14]. Due to the unique features, particularly the narrow energy gap, fullerenes are one of the most appealing families of nanostructures [13–15]. According to a review of literature, the $X_{12}Y_{12}$ (X = Al, B and Y = N, P) structures are the most stable of all the fullerene-like structures [13, 14, 16, 17]. The medical applications of valproic acid (VLA) and its derivatives are numerous. VLA is a fatty acid that has been used to treat epilepsy, mood disorders, migraines, and neuropathic pain [18–21]. Despite its medical benefits, VLA exposure during the pregnancy has been linked to the development of autism [22]. VLA and its derivatives are at the center of medical applications that are used for the treatment of different diseases [18–21, 23]. To avoid adverse effects, it is crucial to detect the presence of the VLA in living creatures and give it properly. The 2D structures of valproic acid (2-propylpentanoic acid) and similar derivatives (2-ethylcarproic acid, 2-methylpentanoic acid and 6-methyloctanoic acid) are presented in Figure 1.

Due to advantageous physico-chemical features, fullerenes have been studied extensively. Since drug detection has serious ramifications, researchers have looked into targeted drug delivery and sensor applications of fullerenes [24, 25]. Fullerenes have been reported to be employed in the hunt for anticancer medication delivery [26, 27]. The major goal of the work is to use density functional theory (DFT) to investigate possibilities of chemical functionalization of Al_{12}/B_{12}-N_{12}/P_{12} with VLA. Figure 2 shows the 2D structures of the pristine nanocages.

The findings will serve as a foundation for future experimental investigations of drug delivery system development.

DFT calculations

The Gaussian 16 program suite was used to do all theoretical computations [28, 29]. Quantum chemistry computations were used to investigate the interaction of VLA with nanocages (NC) with B3LYP/6-311G* basis which is suitable for modeling [30]. To confirm the lowest energy point of all

✉ Jamelah S. Al-Otaibi
jamelah2019@rediffmail.com; jsalotabi@pnu.edu.sa

[1] Department of Chemistry, College of Science, Princess Nourah Bint Abdulrahman University, P.O. Box 84428, Riyadh 11671, Saudi Arabia

[2] Thushara, Neethinagar-64, Pattathanam, Kollam, Kerala, India

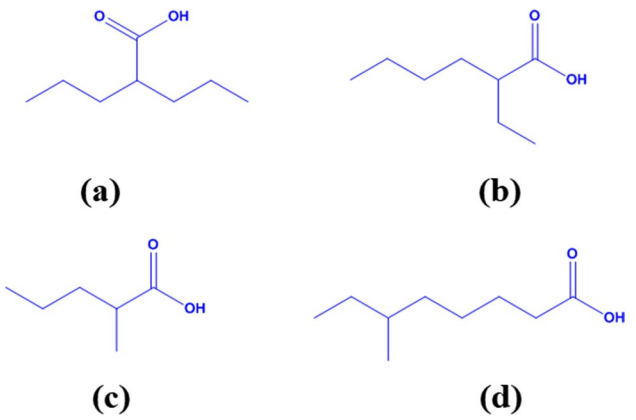

Fig. 1 2D structures of **a** valproic acid (2-propylpentanoic acid), **b** 2-ethylcarproic acid, **c** 2-methylpentanoic acid, and **d** 6-methyloctanoic acid

structures, frequency studies were performed. Chemical descriptors such as energy gap, $E_g = (E_{HOMO} \sim E_{LUMO})/2$; chemical potential, $\mu = (E_{LUMO} + E_{HOMO})/2$; chemical hardness, $\eta = (E_{LUMO} - E_{HOMO})/2$; softness $S = 1/(2\eta)$; and electrophilicity index, $\omega = \mu^2/2\eta$ were calculated [31, 32], where E_{HOMO} and E_{LUMO} are the energies of highest occupied molecular orbital (HOMO) and lowest unoccupied molecular orbitals (LUMO). The adsorption energy was calculated as $E_{ads} = E_{VLA\text{-}NC} - E_{NC} - E_{VLA}$ [33–35], and the conductor-like polarizable continuum model (CPCM) was used to examine solvation effects [36].

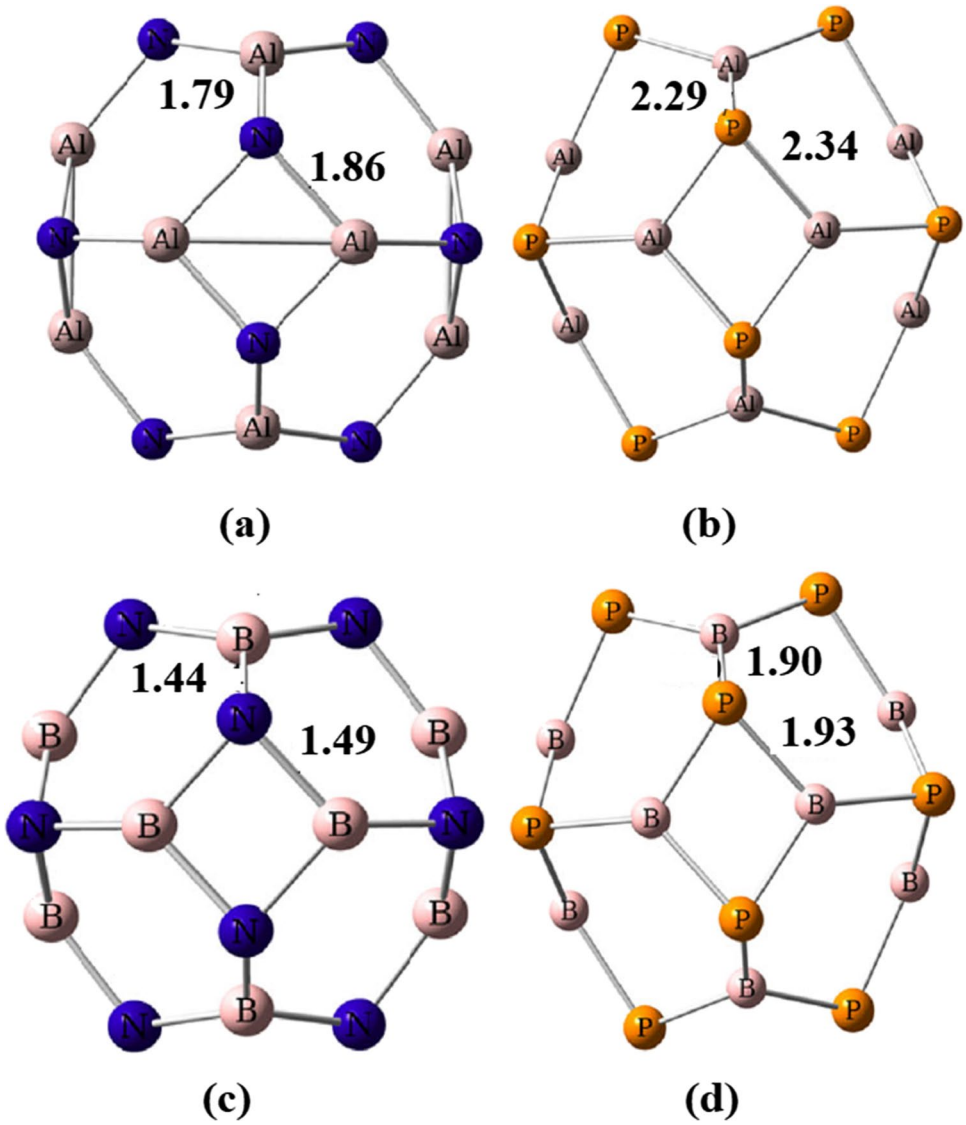

Fig. 2 2D structures of **a** $Al_{12}N_{12}$, **b** $Al_{12}P_{12}$, **c** $B_{12}N_{12}$, and **d** $B_{12}P_{12}$ nanocages

Results and discussion

Properties of nanocages and VLA

The relaxed ground state structures of VLA and all four NCs, as well as their FMOs distribution and molecular electrostatic potential (MEP) plots, are shown in Figures 3 and 4. The equilibrium bond length are Al-N = 1.79, 1.86; Al-P = 2.34, 2.29; B-N = 1.44, 1.49; and B-P = 1.93, 1.90 Å for all pristine cages. The HOMO and LUMO were roughly on the vicinity of N, P and Al, B atoms, as shown in Figure 4. The HOMO and LUMO energies for NCs given in units of eV are (a) $Al_{12}N_{12}$ (−7.1781, −2.5227), (b) $Al_{12}P_{12}$ (−6.8169, −3.4272), (c) $B_{12}N_{12}$ (−7.8594, −1.1050), and (d) $B_{12}P_{12}$ (−6.9600, −3.2278) (Table 1). The band gaps for the NCs in units of eV are (a) $Al_{12}N_{12}$ (4.6554), (b) $Al_{12}P_{12}$ (3.3897), (c) $B_{12}N_{12}$ (6.7544), and (d) $B_{12}P_{12}$ (3.7322). Based on energy gap (E_g) values, $B_{12}N_{12}$ and $Al_{12}P_{12}$ are the least and the most electrically conductive ones. Using values of E_g, the kinetic stability of the NCs may be examined. The chemical descriptor values of relaxed NCs revealed that $Al_{12}P_{12}$ with low kinetic consistency have more reactivity than the others. The HOMO and LUMO energies for VLA were −7.7222 and −0.4177 eV [37, 38].

Interaction of VLA and nanocages

The VLA is coupled to surfaces of Al_{12}/B_{12}-N_{12}/P_{12} via COOH group (Figure 5). The reactive regions of VLA and NCs attached to each other for adsorption process. The values of charges of atoms in VLA interacting with $Al_{12}N_{12}$, $Al_{12}P_{12}$, $B_{12}N_{12}$, and $B_{12}P_{12}$ are −0.531092, −0.424069, −0.436418, and −0.497144 (O1 of COH); −0.330518, −0.442946, −0.280203, and −0.343344 (O2 of C = O); and 0.433564, 0.469323, 0.424040, and 0.437267 (H26 of COH), while that of VLA are −0.560731, −0,384,422, and 0.378393e (Table 2) [13].

Adsorption of VLA on NCs alters the electronic characteristics of both the nanocages and VLA (Tables 1 and 3). The electronic and chemical features of nanocages and complexes were investigated using the value of dipole moment (DM). Significant changes in values are detected after the adsorption process. The DM of isolated nanocages was zero due to symmetry, but it increased after adsorption. The DM values in VLA-NCs are varying from 1.0255 ($B_{12}P_{12}$-VLA) to 7.2774 ($Al_{12}P_{12}$-VLA) Debye. The global reactivity values were crucial for reactivity and stability of VLA, nanocages, and nanocage-VLA complexes. Hardness decreased in VLA-NCs, indicating higher reactivity than that of NCs, allowing for more VLA to be adsorbed (Tables 1 and 3). As a result, the decrease in hardness was followed by an increase in softness and chemical potential. Chemical potential for $Al_{12}N_{12}$, $Al_{12}P_{12}$, $B_{12}N_{12}$, and $B_{12}P_{12}$ NCs changed from −4.8504 to −4.3954, −5.1221 to −4.6930, −4.4822 to −4.2980, and −5.0939 to −5.0654 eV, after adsorption. The highest and the least values of chemical potential shift caused by complexation belong to $Al_{12}N_{12}$ (0.4550 eV) and $B_{12}P_{12}$ (0.0285 eV). The electrophilicity index measures the fragments' capacity to receive electrons [39]. Except for $B_{12}P_{12}$, the electrophilicity index increased with VLA adsorption resulting with a higher tendency to accept electrons. The HOMO plots of the complexes revealed a higher density of electrons around nanocages except $Al_{12}P_{12}$, while LUMO is over the cages except $B_{12}N_{12}$ (Figure 6). Upon the adsorption of VLA on nanoclusters close to the Fermi level, there is seen to be significant change in the location of FMOs distribution in all nanoclusters.

Adsorption of VLA onto NCs caused small modifications in FMOs energies. Energies (eV) of HOMO, LUMO, and E_g for $Al_{12}N_{12}$-VLA ($Al_{12}P_{12}$-VLA) and $B_{12}N_{12}$-VLA ($B_{12}P_{12}$-VLA) systems were calculated −6.1973, −2.5935,

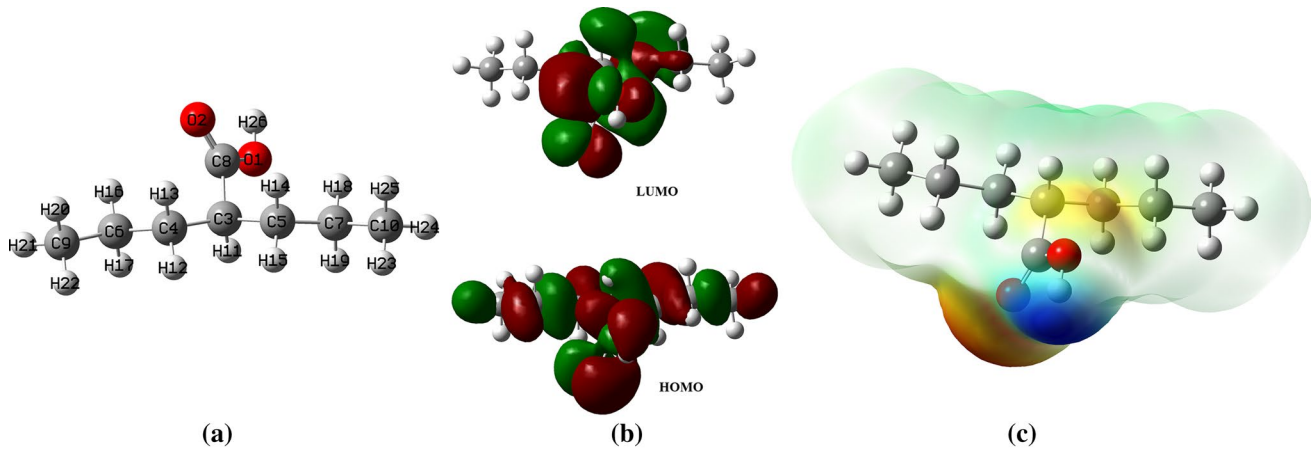

Fig. 3 **a** Optimized geometry of VLA, **b** frontier molecular orbitals (FMOs) plots, and **c** molecular electrostatic potential (MEP) plot

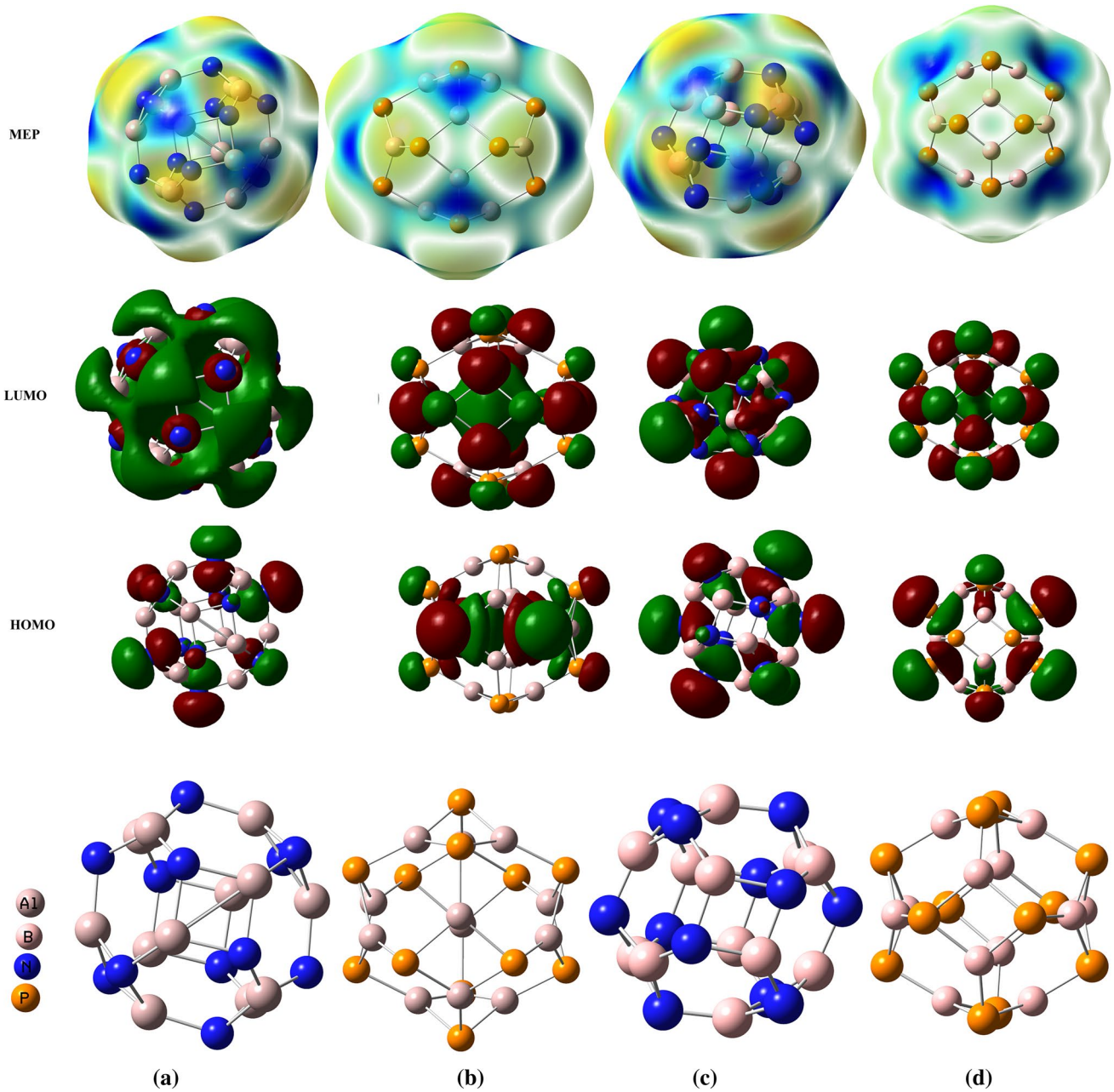

Fig. 4 Optimized geometries, frontier molecular orbitals plots, and molecular electrostatic potential plots of **a** $Al_{12}N_{12}$, **b** $Al_{12}P_{12}$, **c** $B_{12}N_{12}$ (d) $B_{12}P_{12}$

and 3.6038 (and − 6.3165, − 3.0694, 3.2471) and − 7.0262, − 1.5698, and 5.4564 (− 6.9146, − 3.2161, 3.6985), respectively. E_g values of all nanocage-VLA systems were lowered after adsorption and increase conductivity which is suitable for an electrochemical biosensor for VLA [40, 41]. Varying colors, ranging from blue to red, represent different electrostatic potential levels. The positive (blue) and negative (red) regions of MEP are related to electrophilic and nuclophilic reactivity, respectively. The most reactive sites of VLA (Figure 3) and VLA-NCs (Figure 7) are identified as favorable charge transfer and interactions in the adsorption process which is supported by the chemical descriptors and Mulliken charge values. The adsorption energies of VLA onto $Al_{12}N_{12}$, $Al_{12}P_{12}$, $B_{12}N_{12}$, and $B_{12}P_{12}$ NCs were calculated − 144.14, − 109.71, − 105.22, and − 84.96 kcal/mol at the optimum distances. The large negative E_{ads} for VLA adsorption suggested a chemisorption.

The density of states (DOS) plots (Fig. S1) showed how adsorption modifies the electronic characteristics of the nanocages, which may be utilized to estimate their

Table 1 Chemical descriptors of VLA and NCs

Property	VLA	$Al_{12}N_{12}$	$Al_{12}P_{12}$	$B_{12}N_{12}$	$B_{12}P_{12}$
E_{HOMO} (eV)	−7.7222	−7.1781	−6.8169	−7.8594	−6.9600
E_{LUMO} (eV)	−0.4177	−2.5227	−3.4272	−1.1050	−3.2278
E_g (eV)	7.3045	4.6554	3.3897	6.7544	3.7322
Fermi level (eV)	−4.0700	−4.8504	−5.1221	−4.4822	−5.0939
Chemical potential (eV)	−4.0700	−4.8504	−5.1221	−4.4822	−5.0939
Hardness (eV)	3.6523	2.3277	1.6949	3.3772	1.8661
Softness (1/eV)	0.1369	0.2148	0.2950	0.1481	0.2679
Electrophilicity index (eV)	2.2677	5.0536	7.7395	2.9744	6.9524
DM (Debye)	1.4902	0	0	0	0
Polarizability (a.u.)	94.7800	292.6810	613.5573	151.9643	410.6030

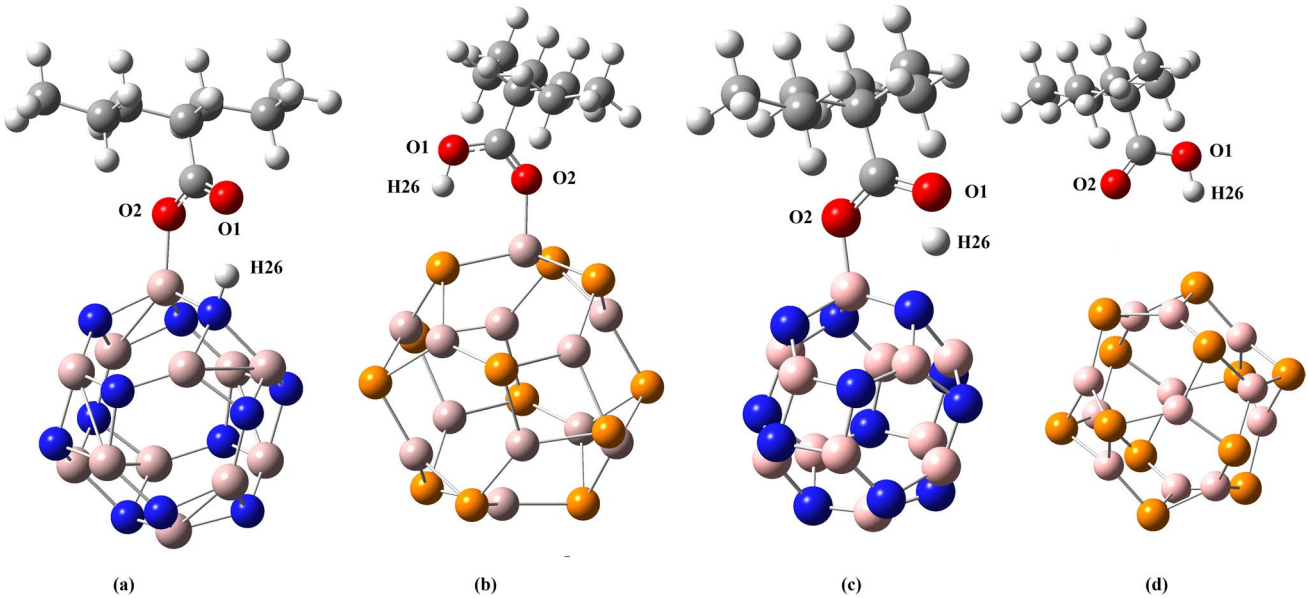

Fig. 5 Optimized geometries of **a** VLA-$Al_{12}N_{12}$, **b** VLA-$Al_{12}P_{12}$, **c** VLA-$B_{12}N_{12}$, and d VLA-$B_{12}P_{12}$

sensitivity to the VLA. The VLA-NC interaction results in new energy levels near to Fermi level and resulted in low E_g values (Fig. S1). The changes in E_g are 1.0516, 0.1426, 1.2980, and 0.0337 eV for complexation of Al_{12}/B_{12}-N_{12}/P_{12}. It can be inferred that for the complexation of $B_{12}N_{12}$ and $B_{12}P_{12}$, the maximum and lowest changes in E_g were observed [42, 43]. Because E_g is a key element in determining a material electrical conductivity, the $B_{12}N_{12}$ system is expected to produce more changes in conductivity after complexation. A decrease in E_g produces larger electrical conductivity: $\sigma \alpha \exp(-E_g/2KT)$ [44]. These findings clearly show that while $Al_{12}N_{12}$ and $Al_{12}P_{12}$ are strong adsorbents for VLA, but they are not the greatest options for making a VLA sensor. However, while $B_{12}N_{12}$ is not the best adsorbent for VLA, it is quite sensitive to it. The findings also suggest that $B_{12}P_{12}$ is a viable candidate for use as a VLA sensor.

The nanocage-VLA structures' thermodynamic properties were also investigated to ensure their thermal stability. Reaction is endothermic if $\Delta H > 0$, exothermic if $\Delta H < 0$, and ΔG tells us whether the VLA and NCs have a spontaneous interaction ($\Delta G < 0$) or not ($\Delta G > 0$). The ΔG and ΔH are given as follows [45, 46]: $\Delta G/H = G/H_{NC\text{-}VLA} - G/H_{NC} - G/H_{VLA}$, where G/H is the Gibbs free energy (G)/enthalpy (H). In the adsorption behavior of the VLA-NC complexes, VLA interacts with NCs, maintaining distances of 1.7992, 2.8629 (O to Al and O to N) for VLA-$Al_{12}N_{12}$; 1.9220, 2.2209 (O to Al and OH to P) for VLA-$Al_{12}P_{12}$; 1.5602, 2.5486 (O to B and OH to N) for VLA-$B_{12}N_{12}$; and 3.6114, 3.8407, 2.6434 Å (O to P, OH to B, and OH to P) for VLA-$B_{12}P_{12}$ systems. The adsorption energies are highest for all systems except $B_{12}P_{12}$-VLA. Furthermore, significant differences in thermodynamic properties were identified for nanocages and

Table 2 Mulliken charges

Atom	VLA	VLA-$Al_{12}N_{12}$	VLA-$Al_{12}P_{12}$	VLA-$B_{12}N_{12}$	VLA-$B_{12}P_{12}$
O1	−0.560731	−0.531097	−0.424069	−0.436418	−0.497144
O2	−0.384422	−0.330518	−0.442946	−0.280203	−0.343344
C3	−0.275644	−0.282228	−0.284642	−0.286427	−0.265944
C4	−0.322307	−0.399891	−0.415465	−0.409100	−0.405663
C5	−0.322280	−0.423527	−0.415437	−0.409368	−0.405191
C6	−0.341586	−0.414817	−0.408842	−0.403168	−0.396584
C7	−0.341591	−0.399876	−0.408853	−0.403102	−0.397055
C8	0.519910	0.462745	0.512177	0.515327	0.439798
C9	−0.518929	−0.621978	−0.618323	−0.616498	−0.614369
C10	−0.518933	−0.620194	−0.618319	−0.616491	−0.614306
H11	0.200684	0.229944	0.244201	0.242565	0.226290
H12	0.175035	0.202266	0.217839	0.215336	0.204066
H13	0.189464	0.219044	0.238217	0.230850	0.217143
H14	0.189481	0.214726	0.238214	0.230841	0.216991
H15	0.175025	0.212242	0.217833	0.215419	0.204001
H16	0.180652	0.230321	0.223462	0.212781	0.207948
H17	0.173591	0.196923	0.206066	0.205727	0.200714
H18	0.180667	0.227612	0.223454	0.212719	0.208131
H19	0.173577	0.200085	0.206063	0.205807	0.200654
H20	0.176851	0.209436	0.217475	0.213320	0.206819
H21	0.176191	0.208677	0.215915	0.215970	0.209171
H22	0.171934	0.203035	0.206508	0.206126	0.202755
H23	0.171928	0.203361	0.206511	0.206147	0.202758
H24	0.176187	0.210058	0.215915	0.215986	0.209184
H25	0.176855	0.205341	0.217467	0.213297	0.206808
H26	0.378393	0.433564	0.469323	0.424040	0.437267

Table 3 Chemical descriptors for the complexes calculated in gas and solvent (water)

Property	VLA-$Al_{12}N_{12}$	VLA-$Al_{12}P_{12}$	VLA-$B_{12}N_{12}$	VLA-$B_{12}P_{12}$
EHOMO (eV)	−6.1973 (−6.2999)	−6.3165 (−6.1546)	−7.0262 (−7.0003)	−6.9146 (−6.5119)
ELUMO (eV)	−2.5935 (−2.2569)	−3.0694 (−2.6433)	−1.5698 (−1.0033)	−3.2161 (−2.7023)
E_g (eV)	3.6038 (4.0430)	3.2471 (3.5113)	5.4564 (5.9970)	3.6985 (3.8096)
Fermi level (eV)	−4.3954 (−4.2784)	−4.6930 (−4.3990)	−4.2980 (−4.0018)	−5.0654 (−4.6071)
Hardness (eV)	1.8019 (2.0215)	1.6236 (1.7557)	2.7282 (2.9985)	1.8493 (1.9048)
Softness (1/eV)	0.2775 (0.2473)	0.3080 (0.2848)	0.1833 (0.1668)	0.2704 (0.2625)
Chemical potential (eV)	−4.3954 (−4.2784)	−4.6930 (−4.3990)	−4.2980 (−4.0018)	−5.0654 (−4.6071)
Electrophilicity index (eV)	5.3609 (4.5275)	7.7824 (5.5108)	3.3855 (2.6704)	6.9372 (5.5715)
DM (Debye)	2.7098 (3.8107)	7.2774 (9.2743)	6.3482 (7.7125)	1.0255 (1.9339)
Polarizability (a.u.)	390.9723 (580.1210)	726.7756 (1409.0643)	257.6080 (377.4406)	515.5046 (961.5546)

the VLA-NC complex (Tables 4 and 5). The negative values of the above suggest exothermic, spontaneous, and thermodynamically ordered interactions. The frequencies of all systems are positive, indicating that the examined VLA-NC clusters studied occur naturally [47–51].

Solvation energies

In solution phase, the total energy values of nanocage-VLA are higher than that in the gaseous phase. This shows the examined complex's stability if higher in the

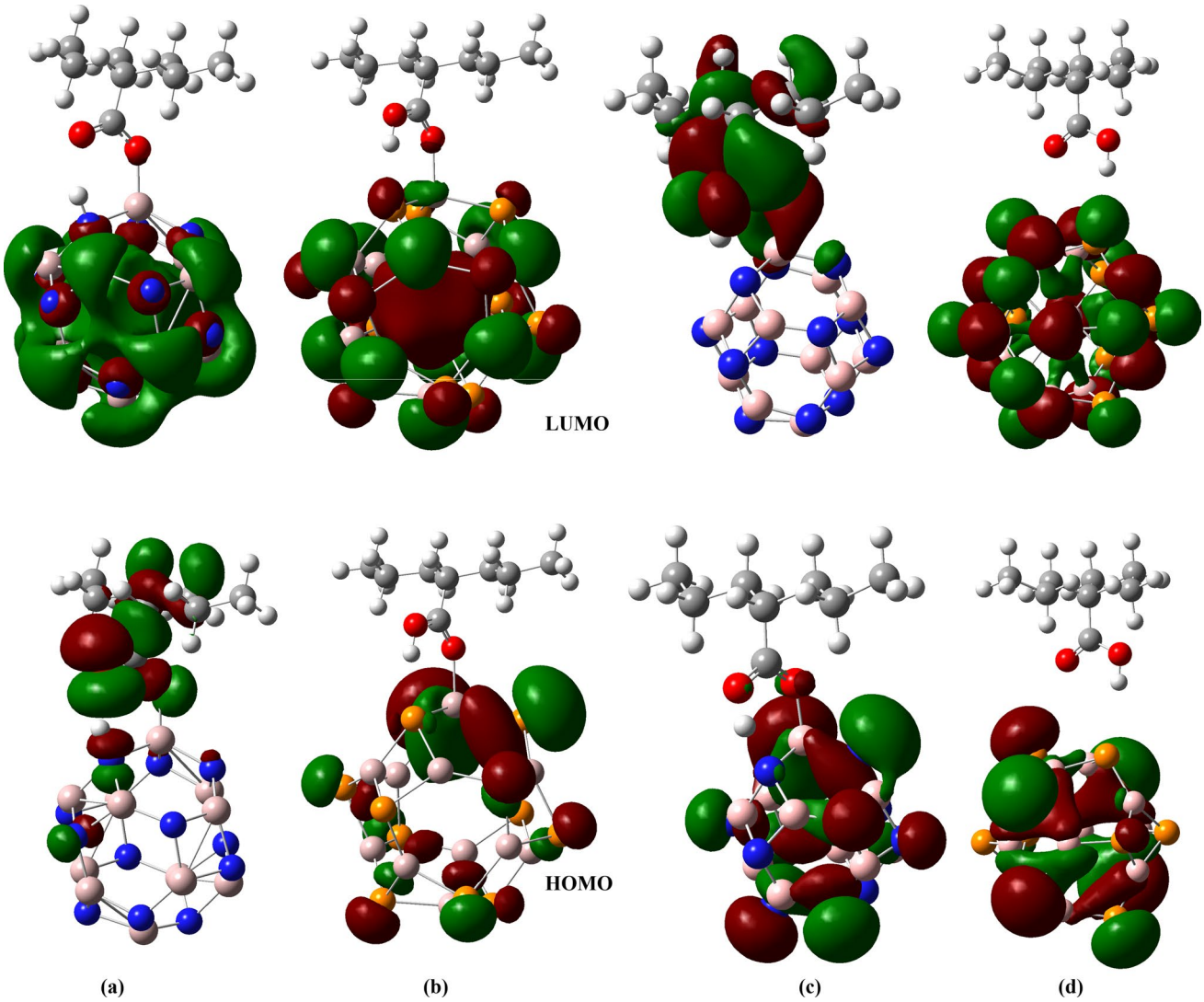

Fig. 6 HOMO–LUMO plots of **a** VLA-$Al_{12}N_{12}$, **b** VLA-$Al_{12}P_{12}$, **c** VLA-$B_{12}N_{12}$, and **d** VLA-$B_{12}P_{12}$

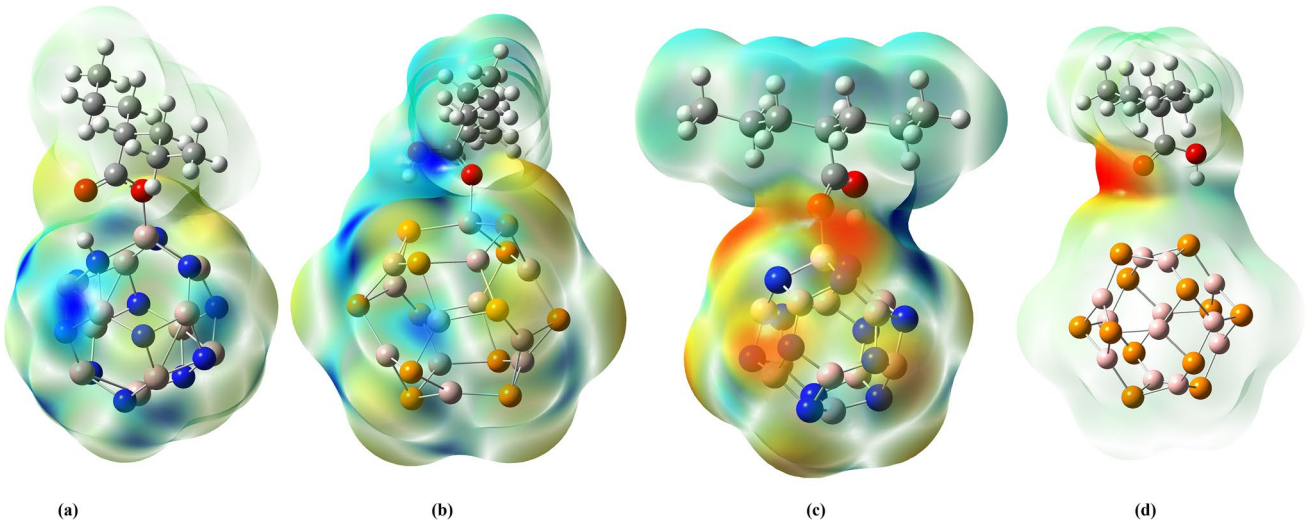

Fig. 7 MEP plots of **a** VLA-$Al_{12}N_{12}$, **b** VLA-$Al_{12}P_{12}$, **c** VLA-$B_{12}N_{12}$, **d** VLA-$B_{12}P_{12}$

Table 4 Thermochemical (thermodynamic) quantities

Compounds	E/Hartree	H/Hartree	G/Hartree	S/cal/mol K
VLA	− 464.713963	− 464.700517	− 464.754008	112.581
$Al_{12}N_{12}$	− 3567.559815	− 3567.538483	− 3567.604394	138.720
$Al_{12}P_{12}$	− 7006.756850	− 7006.722940	− 7006.816434	196.774
$B_{12}N_{12}$	− 956.212430	− 956.201377	− 956.247316	96.688
$B_{12}P_{12}$	− 4394.912764	− 4394.889848	− 4394.956779	140.869
Gaseous phase				
VLA-$Al_{12}N_{12}$	− 4032.502568	− 4032.467233	− 4032.567416	210.853
VLA-$Al_{12}P_{12}$	− 7471.643894	− 7471.596248	− 7471.722815	266.384
VLA-$B_{12}N_{12}$	− 1421.093560	− 1421.069040	− 1421.147595	165.333
VLA$B_{12}P_{12}$	− 4859.761784	− 4859.723918	− 4859.835292	234.407
Water (solvent)				
VLA-$Al_{12}N_{12}$	− 4032.561110	− 4032.527040	− 4032.621532	198.875
VLA-$Al_{12}P_{12}$	− 7471.682466	− 7471.637230	− 7471.757034	252.149
VLA-$B_{12}N_{12}$	− 1421.123953	− 1421.100070	− 1421.175654	159.080
VLA$B_{12}P_{12}$	− 4859.783702	− 4859.747681	− 4859.849936	215.214

Table 5 Changes of the thermochemical quantities

Compounds	Δ*E*/kcal/mol	Δ*H*/kcal/mol	Δ*G*/kcal/mol	*S*/cal/mol K
Gaseous phase				
VLA-$Al_{12}N_{12}$	− 143.57	− 143.22	− 131.16	− 40.448
VLA-$Al_{12}P_{12}$	− 108.61	− 108.43	− 95.62	− 42.971
VLA-$B_{12}N_{12}$	− 104.90	− 104.89	− 91.79	− 43.936
VLA$B_{12}P_{12}$	− 84.75	− 83.81	− 78.13	− 19.043
Water (solvent)				
VLA-$Al_{12}N_{12}$	− 180.30	− 180.75	− 165.12	− 52.426
VLA-$Al_{12}P_{12}$	− 132.81	− 134.14	− 117.09	− 57.206
VLA-$B_{12}N_{12}$	− 123.97	− 124.36	− 109.39	− 50.189
VLA$B_{12}P_{12}$	− 98.50	− 98.72	− 87.32	− 38.236

solution phase than in the gas phase. The solvation energy, SFE = $E_{solvent} - E_{gas}$. The solvation energies are − 179.23, − 131.66, − 122.48, and − 98.00 kcal/mol for $Al_{12}N_{12}$, $Al_{12}P_{12}$, $B_{12}N_{12}$, and $B_{12}P_{12}$ with VLA systems. For all systems in the solvent water, the thermodynamic parameter changes are negative showing the processes as spontaneous and exothermic (Tables 4 and 5). In solution phase, the DM values (Table 3) of the complex increase, which is due to long range interactions of the solvent with the solute molecule. In solution phase, the complex's polarizability values are higher and the stability of HOMO and LUMO rises and the high energy gap indicate that energy is transferred efficiently between them. The E_g value in solution phase increases as compared to the gaseous phase which reveals that the nanocages are set to share electrons (Table 3). The change in E_g of VLA-NC structures in solvents was also calculated as 0.6124/0.1216/0.7574/0.0774 eV for VLA-$Al_{12}N_{12}$/$Al_{12}P_{12}$/$B_{12}N_{12}$/$B_{12}P_{12}$ and discussed in order to nominate an electrical sensor for the VLA. In VLA-NC clusters, energy gap increases in all solvents. It means the nanocages are good sensors as supported by its solvation or adsorption energies. This is also evident from the Raman spectra (Fig. S2) in which in the finger print regions, maximum enhancements are for VLA-NC clusters due to SERS effects [47, 52]. Most of the modes are enhanced in complexes due to the interaction between VLA and nanocages.

Conclusion

DFT computations were used to study adsorption of valproic acid on Al_{12}/B_{12}-N_{12}/P_{12} nanocages. The chemical descriptors and electronic features are modified due to the adsorption process. The drug was attached to the nanocages via the COOH groups' oxygen and hydrogen atoms with reasonable adsorption energies. VLA-$Al_{12}N_{12}$ and VLA-$B_{12}P_{12}$ have the highest and the least values of chemical potential shift. Although $Al_{12}N_{12}$ and $Al_{12}P_{12}$ are strong adsorbents for VLA, the conductivity values indicate that they are not the best options for building a VLA sensor. $B_{12}N_{12}$ on the

other hand is not the best adsorbent for VLA, but is quite sensitive to it. $B_{12}P_{12}$ appears to be a viable candidate for use as a VLA sensor, according to the findings. The exothermic nature of process was demonstrated by negative adsorption energies and thermodynamic parameters. The adsorption energies of VLA are − 144.14, − 109.71, − 105.22, and − 84.96, and the solvation energies in water are − 179.23, − 131.66, − 122.48, and − 98.00 kcal/mol in $Al_{12}N_{12}$, $Al_{12}P_{12}$, $B_{12}N_{12}$, and $B_{12}P_{12}$ nanocages, respectively. Most reactive sites are identified which are suitable for adsorption and charge transfer.

Supplementary Information The online version contains supplementary material available at https://doi.org/10.1007/s00894-022-05088-w.

Acknowledgements The authors express their gratitude to Princess Nourah Bint Abdulrahman University Researchers Supporting Project number (PNURSP2022R13), Princess Nourah bint Abdulrahman University, Riyadh, Saudi Arabia.

Author contribution Jamelah S. Al-Otaibi: software, supervision, manuscript preparation and data analysis. Y. Sheena Mary: supervision, manuscript preparation, conceiving the problem and data analysis. Y. Shyma Mary: manuscript preparation, conceiving the problem, and data analysis and correction.

Data availability The supplementary information files include additional materials.

Code availability No new codes have been created. Existing codes were utilized and quoted correctly.

Declarations

Conflict of interest The authors declare no competing interests.

References

1. Beheshtian J, Peyghan AA, Noei M (2013) Sensing behavior of Al and Si doped BC3 graphenes to formaldehyde. Sens Actuators, B Chem 181:829–834. https://doi.org/10.1016/j.snb.2013.02.086
2. Rad AS, Samipour V, Movaghgharnnezhad S, Mirabi A, Shahavi MH, Moghadas BK (2019) X12N12 (X=Al, B) cluster for protection of vitamin C: molecular modeling investigation. Surface Interfaces 15:30–37. https://doi.org/10.1016/j.surfin.2019.02.001
3. Almuqrin AH, Al-Otaibi JS, Mary YS, Mary YS, Thomas R (2021) Structural study of letrozole and metronidazole and formation of self assembly with graphene and fullerene with the enhancement of physical, chemical and biological activities. J Biomol Struct Dyn 39:5509–5515. https://doi.org/10.1080/07391102.2020.1790420
4. Al-Otaibi JS, Mary YS, Thomas R, Kaya S (2020) Detailed electronic structure, physico-chemical properties, excited state properties, virtual bioactivity screening and SERS analysis of three guanine based antiviral drugs, valacyclovir HCl hydrate, Acyclovir and ganciclovir. Polycyclic Aromat Compd. https://doi.org/10.1080/10406638.2020.1773876
5. Al-Otaibi JS, Mary YS, Mary YS, Kaya S, Erkan S (2020) Spectral analysis and DFT investigation of some benzopyran analogues and their self assemblies with graphene. J Mol Liq 317:113924. https://doi.org/10.1016/j.molliq.2020.113924
6. Rad AS, Ayub K (2017) Adsorption properties of acetylene and ethylene molecules onto pristine and nickel decoarated Al12N12 nanoclsuters. Mater Chem Phys 194:337–344. https://doi.org/10.1016/j.matchemphys.2017.04.002
7. Rad AS, Ayub K (2017) DFT study of boron trichloride adsorption on the surface of Al12N12 nanocluster. Mol Phys 115:879–884. https://doi.org/10.1080/00268976.2017.1290843
8. Velammal SP, Devi TA, Amaladhas TP (2016) Antioxidant, antimicrobial and cytotoxic activities of silver and gold nanoparticle ssynthesized using plumbago zylanica bark. J Nanostruct Chem 6:247–260. https://doi.org/10.1007/s40097-016-0198-x
9. Goodarzi Z, Maghrebi M, Zavareh AF, Mokhtari-Hosseini ZB, Ebrahimi-Hoseinzadeh B, Zarmi AH, Barshan-Tashnizi M (2015) Evaluation of nicotine sensor based on copper nanoparticles and carbon nanotubes. J Nanostruct Chem 5:237–242. https://doi.org/10.1007/s40097-015-0154-1
10. Harismah K, Mirzaei M, Samadizadeh M, Rad AS (2017) DFT studies of stabilities and properties for X3Y6Z9 borazine like structures (X=B/Al, Y-N/P, Z=H/Me). Superlattices Microstruct 109:360–365. https://doi.org/10.1016/j.spmi.2017.05.027
11. Jafari Z, Baharfar R, Rad AS, Asghari S (2020) Potential of graphene oxide as a drug delivery system for sumatriptan: a detailed density functional theory study. J Biomol Struct Dyn. https://doi.org/10.1080/07391102.2020.1736161
12. Khodashenas B, Ardjmand M, Mazyar SB, Rad AS, Khiyavi AA (2019) Bovine serum albumin/gold nanoparticles as a drug delivery system for curcumin: experimental an dcomputational studies. J Biomol Struct Dyn. https://doi.org/10.1080/07391102.2019.1683073
13. Padash R, Rahimi-Nasrabadi M, Rad AS, Sobhani-Nasab A, Jesionowski T, Ehrlich H (2019) A comparative computational investigation of phosgene adsorption on (XY)12 (X=Al, B and Y=N, P) nanoclusters: DFT investigations. J Cluster Sci 30:203–218. https://doi.org/10.1007/s10876-018-1479-y
14 Padash R, Sobhani-Nasab A, Rahimi-Nasrabadi M, Mirmotahri M, Enrlich H, RAd AS, Peyravi M (2018) Is it possible to use X12Y12 (X=Al, B and Y=N, P) nanocages for drug delivery systems? A DFT study on the adsorption property of 4-aminopyriidne drug. Appl Phys A 124:582. https://doi.org/10.1007/s00339-018-1965-y
15. Sherfati M, Rad AS, Ardjmand M, Heydarinasab A, Peyravi M, Mirzaei M (2018) Beryllium oxide (BeO) nanotube provides excellent surface towards adenine adsorption: a dispersion-corrected DFT study in gas and water phases. Curr Appl Phys 18:1059–1065. https://doi.org/10.1016/j.cap.2018.05.024
16. Strout DL (2000) Structure and stability of boron nitrides: isomers of B12N12. J Phys Chem A 104:3364–3366. https://doi.org/10.1021/jp994129a
17. Wang R, Zhang D, Liu C (2005) Theoretical prediction of a novel inorganic fullerene like family of silicon carbon materials. Chem Phys Lett 411:333–338. https://doi.org/10.1016/j.cplett.2005.06.055
18. Loscher W (2002) Basic pharmacology of valproate: a review after 35 years of clinical use for the treatment of epilepsy. CNS Drugs 16:669–694. https://doi.org/10.2165/00023210-200216100-00003
19. Waszkielewicz AM, Gunia A, Sloczynska K, Marona H (2011) Evaluation of anticonvulsants for possible use in neuropathic pain. Curr Med Chem 18:4344–4358. https://doi.org/10.2174/092986711797200408
20. Chiu CT, Wang Z, Hunsberger JG, Chuang DM (2013) Therapeutic potential of mood stabilizers lithium and valproic acid: beyond bipolar disorder. Pharmacol Rev 65:105–142. https://doi.org/10.1124/pr.111.005512

21. Hoffmann J, Akerman S, Goadsby PJ (2014) Efficacy and mechanism of anticonvulsant drugs in migraine. Expert Rev Clin Pharmacol 7:191–201. https://doi.org/10.1586/17512433.2014.885835
22. Ornoy A (2009) Valproic acid in pregnancy: how much are we endangering the embryo and fetus? Reprod Toxicol 28:1–10. https://doi.org/10.1016/j.reprotox.2009.02.014
23. Alver O, Parlak C, Senyel M, Ramasami P (2018) Density functional theory study on the adsorption of valproic acid to doped fullerenes. Main Group Met Chem 41:67–71. https://doi.org/10.1515/mgmc-2018-0002
24. Da Ros T (2008) Twenty years of promises: Fullerene in medicinal chemistry. In: F Cata; dp. T Da Ros (eds), Medicinal chemistry and pharmacological potential of fullerenes and carbon nanotubes, Carbon Materials: Chemistry and Physics, vol.1, Springer, Dordrecht, https://doi.org/10.1007/978-1-4020-6845-4_1
25. Singh R, Lillard JW (2009) Nanoparticle based targeted drug delivery. Exp Mol Pathol 86:215–223. https://doi.org/10.1016/j.yexmp.2008.12.004
26. Zakharian TY, Seryshev A, Sithraman B, Gilbert BE, Knight V, Wilson LJ (2005) A fullerene paclitaxel chemotherapeutic: synthesis, characterization and study of biological activity in tissue culture. J Am Chem Soc 127:12508–12509. https://doi.org/10.1021/ja0546525
27. Ashcroft JM, Tsyboulski DA, Hartman KB, Zakharian TY, Marks JW, Weisman RB, Rosenblum MG, Wilson LJ (2006) Fullerene (C60) immunoconjugates: interaction of water soluble C60 derivatives with the murine anti-gp240 melanoma antibody. Chem Commun (Camb) 28:3004–3006. https://doi.org/10.1039/B601717G
28. Gaussian 16, Revision A.03, M.J. Frisch, G.W. Trucks, H.B. Schlegel, G.E. Scuseria, M.A. Robb, J.R. Cheeseman, G. Scalmani, V. Barone, G.A. Petersson, H. Nakatsuji, X. Li, M. Caricato, A.V. Marenich, J. Bloino, B.G. Janesko, R. Gomperts, B. Mennucci, H.P. Hratchian, J.V. Ortiz, A.F. Izmaylov, J.L. Sonnenberg, D. Williams-Young, F. Ding, F. Lipparini, F. Egidi, J. Goings, B. Peng, A. Petrone, T. Henderson, D. Ranasinghe, V.G. Zakrzewski, J. Gao, N. Rega, G. Zheng, W. Liang, M. Hada, M. Ehara, K. Toyota, R. Fukuda, J. Hasegawa, M. Ishida, T. Nakajima, Y. Honda, O. Kitao, H. Nakai, T. Vreven, K. Throssell, J.A. Montgomery, Jr., J.E. Peralta, F. Ogliaro, M.J. Bearpark, J.J. Heyd, E.N. Brothers, K.N. Kudin, V.N. Staroverov, T.A. Keith, R. Kobayashi, J. Normand, K. Raghavachari, A.P. Rendell, J.C. Burant, S.S. Iyengar, J. Tomasi, M. Cossi, J.M. Millam, M. Klene, C. Adamo, R. Cammi, J.W. Ochterski, R.L. Martin, K. Morokuma, O. Farkas, J.B. Foresman, and D. J. Fox, Gaussian, Inc., Wallingford CT, 2016.
29. GaussView, Version 6.1, R.Dennington, T.A.Keith, J.M.Millam, Semichem Inc., Shawnee Mission, KS, 2016.
30. Mahboobeh K, Elham TL (2020) B12Y12 (Y:N, P) fullerene like cages for emestane-delivery; molecular modeling investigation. J Mol Struct 1217:128455. https://doi.org/10.1016/j.molstruc.2020.128455
31. Parr RG, Szentpaly LV, Liu S (1999) Electrophilicity index. J Am Chem Soc 121:1922–1924. https://doi.org/10.1021/ja983494x
32. Fuentealba P, Simon-Manso Y, Chattaraj PK (2000) Molecular electronic excitations and the minimum polarizability principle. J Phys Chem A 104:3185–3187. https://doi.org/10.1021/jp992973v
33. Padash R, Esfahani MR, Rad AS. The computational quantum mechanical study of sulfamide drug adsorption ontoX12Y12 fullerene like nanocages: detailed DFT and QTAIM investigations. J Biomol Struct Dyn. https://doi.org/10.1080/07391102.2020.1292991
34. Mary YS, Kumar VS, Mary YS, Resmi KS, Thomas R (2020) Detailed quantum mechanical studies on three bioactive benzimidazole derivatives and their Raman enhancement on adsorption over graphene sheets. Polycyclic Aromat Compd. https://doi.org/10.1080/10406638.2020.1852267
35. Al-Otaibi JS, Almuqrin AH, Mary YS, Mary YS (2020) Utilization of O/S-doped graphene nanoclusters for ultrasensitive detection of flurane derivatives-DFT investigations. J Biomol Struct Dyn. https://doi.org/10.1080/07391102.2020.1870155
36. Cossi M, Rega N, Scalmani G, Barone V (2003) Energies, structures, and electronic properties of molecules in solution with the C-PCM solvation model. J Comp Chem 24:669–681. https://doi.org/10.1002/jcc.10189
37. Almuqrin AH, Al-Otaibi JS, Mary YS, Thomas R, Kaya S, Isin DO (2020) Spectral analysis and detailed quantum mechanical investigation of some acetanilide analogues and their self assemblies with graphene and fullerene. J Mol Model 26:254. https://doi.org/10.1007/s00894-020-04485-3
38. Al-Otaibi JS, Almuqrin AH, Mary YS, Mary YS, Van Alsenoy C (2020) DFT and molecular docking studies of self-assembly of sulfone analogues and graphene. J Mol Model 26:273. https://doi.org/10.1007/s00894-020-04546-7
39 O'boyle NM, Tenderholt AL, Langner KM (2008) CClib: a library for package independent computational chemistry algorithms. J Comput Chem 29:839–845. https://doi.org/10.1002/jcc.20823
40. Al-Otaibi JS, Almuqrin AH, Mary YS, Mary YS, Thomas R (2020) Modeling the conformational preference, spectral analysis and other quantum mechanical studies on three bioactive aminobenzoate derivatives and their SERS active graphene complexes. Polycyclic Aromat Compd. https://doi.org/10.1080/10406638.2020.1827270
41. Mary YS, Mary YS, Armakovic S, Armakovic SJ, Narayana B (2020) Understanding reactivity of a triazole derivative and its interaction with graphene and doped/undoped coronene- a DFT study. J Biomol Struct Dyn. https://doi.org/10.1080/07391102.2020.1837677
42. Almuqrin AH, Al-Otaibi JS, Mary YS, Mary YS (2021) DFT computational study towards investigating psychotropic drugs, promazine and trifluoperazine adsorption on graphene, fullerene and carbon cyclic ring nano clusters. Spectrochim Acta 246:119012. https://doi.org/10.1017/j.saa.2020.119012
43. Al-Otaibi JS, Mary YS, Mary YS, Serdaroglu G (2021) Adsorption of adipic acid in Al/B-N/P nanocages: DFT investigations. J Mol Model 27:113. https://doi.org/10.1007/s00894-021-04742-z
44. Al-Otaibi JS, Mary YS, Mary YS, Kaya S, Serdaroglu G (2020) DFT computational study of trihalogenated aniline derivative's adsorption onto graphene/fullerene/fullerene-like nanocages, X12Y12 (X=Al, B and Y=N, P). J Biomol Struct Dyn. https://doi.org/10.1080/07391102.2021.1914172
45. Rad AS (2015) First principles study of Al-doped graphene as nanostructure adsorbent for NO2 and N2O: DFT calculations. Appl Surf Sci 357:1217–1224. https://doi.org/10.1016/j.apsusc.2015.09.168
46. Zou M, Zhang J, Chen J, Li X (2012) Simulating adsorption of organic pollutants on finite (8,0) single walled carbon nanotubes in water. Environ Sci Technol 46:8887–8894. https://doi.org/10.1021/es301370f
47. Al-Otaibi JS, Mary YS, Mary YS (2022) Adsorption of a thione bioactive derivative over different silver/gold clusters – DFT investigations. Comput Theor Chem 1207:113497. https://doi.org/10.1016/j.comptc.2021.113497
48. Al-Otaibi JS, Mary YS, Mary YS, Ullah Z, Yadav R, Gupta N, Churchill DG (2021) Adsorption properties of dacarbazine with graphene/fullerene/metal nanocages-reactivity, spectroscopic and SERS analysis. Spectrochim Acta 120677. https://doi.org/10.1016/j.saa.2021.120677
49. Mary YS, Mary YS, Ullah Z (2021) Computational study of sorbic acid drug adsorption onto coronene/fullerene/fullerene-like X12Y12 (X=Al, B and Y=N, P) nanocages: DFT and molecular docking investigations. J Cluster Sci. https://doi.org/10.1007/s10876-021-02106-4

50. Al-Otaibi JS, Mary YS, Mary YS, Thomas R (2022) Evidence of cluster formation of croconic acid with Ag, Au and Cu cages, enhancement of electronic properties and Raman activity. Spectrochim Acta 264:120233. https://doi.org/10.1016/j.saa.2021.120233
51. Al-Otaibi JS, Mary YS, Mary YS, Trivedi R, Chakraborty B (2021) Theoretical investigation on the adsorption of melamine in Al12/B12-N12/P12 fullerene-like nanocages: a platform for ultrasensitive detection of melamine. Chem Pap. https://doi.org/10.1007/s11696-021-01849-8
52. Al-Otaibi JS, Mary YS, Mary YS, Ullah Z, Kwon HW (2022) Adsorption behavior and solvent effects of an adamantane-triazole derivative on metal clusters-DFT simulation studies. J Mol Liq 345:118242. https://doi.org/10.1016/j.molliq.2021.118242